Analysis and Modeling of the Radial Force in a Switched Reluctance Motor with Sinusoidal Excitations

Feng-Chieh Lin*, Sheng-Ming Yang
Department of Mechanical and Electro-mechanical Engineering
Tamkang University, Tamsui
Taipei County, Taiwan 25137
Tel: 886-2-86314971
Fax: 886-2-26209745
Email: 890340028@s90.tku.edu.tw

Abstract—**Due to its special structure, the shaft radial force and torque of three-phase 12/8 switched reluctance motors can be independently controlled by proper distribution of currents at each pole of the excited phase. Radial force control is useful in balancing: 1) external force acting on the motor shaft, and 2) the imbalanced shaft force due to rotor eccentricity, so as to reduce motor vibrations. In this paper, the radial force and torque produced by the SRM under sinusoidal excitations are analyzed, and a scheme to produce the desired radial force is proposed. It was found that when excited with sinusoidal currents, the SRM can generate the desired shaft radial force in any direction in the rotational plane without interfering with the rotational torque. The scheme was verified with a finite-element analysis software and with an experimental system. Static experiments were performed, and the results have verified the effectiveness of the proposed scheme in controlling radial force of the SRM.**

Keywords — **SRM, radial force, finite-element analysis, sinusoidal excitations.**

I. INTRODUCTION

Switched reluctance motors (SRM) develop torque through an interaction between the electromagnetic excitation from the stator poles and the rotor teeth. Once a particular combination of phase currents is established and maintained in the stator, the rotor teeth will be attracted into an alignment with the stator poles in a particular position. This attracting force can be separated into a tangential and a radial force component. The tangential force converts to the rotational torque of the motor. The net radial force is generally zero due to the geometrical balance of motor structure.

Unbalanced radial force acting on rotor shaft is undesirable since it causes motor vibrations. For instance, in the applications where the external load is not balanced, or when the rotor is not centered and caused non-uniform air gap, shaft radial force exists [1-2]. Due to its special structure and the way torque is produced SRM offers a unique opportunity for controlling shaft radial force without intervening the normal rotational torque productions [3-5]. Radial force control is feasible for SRMs with some particular stator/rotor combinations. For example, 12/8 pole SRM has four stator poles per phase, and when a phase is excited, each pole produces a radial force that is 90 degrees from the adjacent poles in space. Therefore, if the excitation current in each pole can be controlled independently, then the rotational torque and radial force of 12/8 pole SRM can be controlled.

Moreover, because radial force is a function of rotor position, the excitation current must also vary with rotor position in order to achieve radial force control. There were a number of papers discussed the use of sinusoidal current waveforms to control SRM. For example, the vector control scheme commonly used in ac motor drives was adopted to control a three phase SRM [7-8]. However, their objectives were mainly for torque ripple reduction, and not radial force control.

In this paper, a sinusoidal current excitation scheme is proposed for the torque and radial force control of 12/8 pole SRMs. By proper distribution of pole currents in the excited phase the desired motor torque and radial force can be produced.

II. RADIAL FORCE AND TORQUE ANALYSIS

Figure 1 shows the schematic of the 12/8 pole switched reluctance motor discussed in this paper. Only the windings of phase A are shown, and it is assumed that the currents in all the currents in 12 stator poles can be controlled independently. Let phase A be the excited phase, the pole currents are i_{A1}, i_{A2}, i_{A3}, and i_{A4}, respectively, and θ_r is the rotor angle. The stroke angle of this SRM is 15 mechanical degrees. The torque and radial force in the motor can be analyzed by considering the force generated with a single pole, as shown in Fig. 2. As shown in the figure, the flux passes through the overlap area as well as the non-overlap area due to the fringing effect. The inductance can be expressed as [6]

$$L_A = \frac{\mu_0 N^2 L R \theta_o}{2g} + N^2 K_f \theta_{uo} \qquad (1)$$

where μ_o is the permeability of air, K_f is a constant for the fringing inductance, N is the number of coil turns, L is the motor stacking length, R is the rotor radius, g is the air gap length, θ_o and θ_{uo} are the overlapping and the non-overlapping angle, respectively. The radial force F_{A1} and torque T_{A1} in this pole can be expressed as,

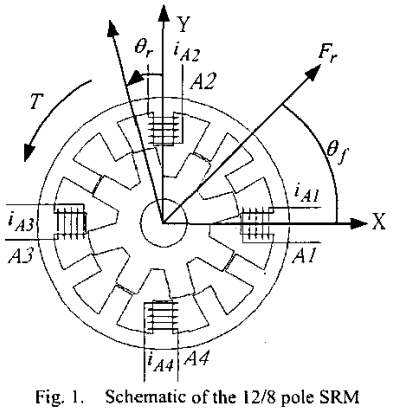

Fig. 1. Schematic of the 12/8 pole SRM

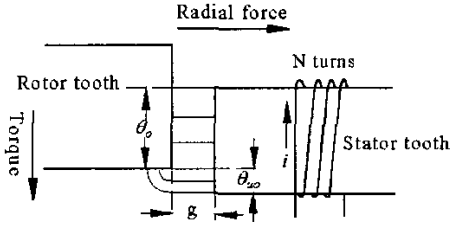

Fig. 2. Pole *A1* of the SRM shown in Fig. 1

$$F_{A1} = \frac{1}{2} i_{A1}^2 \frac{dL_A}{dx} \tag{2}$$

$$T_{A1} = \frac{1}{2} i_{A1}^2 \frac{dL_A}{d\theta_o} \tag{3}$$

Since g is fixed, by neglecting the fringing flux F_{A1} can be simplified as

$$F_{A1} \approx \frac{1}{2} i_{A1}^2 \frac{L_A}{g} \approx \frac{\mu_0 N^2 i_{A1}^2 LR\theta_o}{2g^2} = K_F i_{A1}^2 \tag{4}$$

where $K_F = \frac{\mu_0 N^2 LR\theta_o}{2g^2}$. The above equation shows that the amplitude of the radial force is approximately proportional to the square of the excitation current, and is inversely proportional to the squared air gap length. Also, it is a function of the rotor angle.

When all four poles in phase A are considered, the net radial force can be found by the vector sum of the forces produced by each pole. From Fig. 1, the net radial force in the horizontal and the vertical direction is

$$F_x = F_{A1} - F_{A3} = K_F\left(i_{A1}^2 - i_{A3}^2\right) \tag{5}$$

$$F_y = F_{A4} - F_{A2} = K_F\left(i_{A2}^2 - i_{A4}^2\right) \tag{6}$$

Similarly, the net torque can be found by summing the torque generated by each pole. Because the coil turns and the air gap length are the same for all poles, the motor torque can be written as

$$T = \frac{1}{2}(i_{A1}^2 + i_{A2}^2 + i_{A3}^2 + i_{A4}^2)\frac{dL_A}{d\theta_o} \tag{7}$$

Since T is proportional to the sum of current squared, it is convenient to let $i_{A1}^2 + i_{A2}^2 + i_{A3}^2 + i_{A4}^2 = 4(i_T)^2$, where i_T is the equivalent motor "torque current".

It can be seen from Eqs. (5)-(7) that F_x, F_y and T can be manipulated with proper selection of $i_{A1} \sim i_{A4}$. However, given the desired F_x, F_y and T, there are four unknowns, i.e. $i_{A1} \sim i_{A4}$, to be determined from only three equations. This means that there are infinite number of current combinations that will yield the desired F_x, F_y and T. In this paper, we proposed to use sinusoidal excitation currents for $i_{A1} \sim i_{A4}$ so that the direction of the radial force can be included in the calculation with ease. Consequently, the solutions of Eqs. (5)-(7) become unique because $i_{A1} \sim i_{A4}$ are constrained to sinusoidal waveforms.

III. Sinusoidal Excitation

Since polarities of winding currents have no effect on either motor torque or radial force, it is convenient to express the sinusoidal winding currents as follows

$$i_{A1} = C + K\cos(\theta_f) \tag{8}$$

$$i_{A2} = C + K\sin(\theta_f) \tag{9}$$

$$i_{A3} = C - K\cos(\theta_f) \tag{10}$$

$$i_{A4} = C - K\sin(\theta_f) \tag{11}$$

where θ_f, K, C are the angle, amplitude, and dc offset of the sinusoidal currents. With the above definitions and the desired F_x, F_y and T, the unknowns become θ_f, K, and C. Substituting Eqs. (8)-(11) into Eqs. (5)-(7) gives

$$F_x = 4K_F KC\cos(\theta_f) \tag{12}$$

$$F_y = 4K_F KC\sin(\theta_f) \tag{13}$$

$$\begin{aligned} 4i_T^2 = {} & (C + K\cos(\theta_f))^2 + (C + K\sin(\theta_f))^2 \\ & + (C - K\cos(\theta_f))^2 + (C - K\sin(\theta_f))^2 \end{aligned} \tag{14}$$

It can be seen from Eqs.(12)-(13) that the angle of the radial force is θ_f also. That is, the direction of the radial force is the same as the direction of the winding current. To simply the above results, let the amplitude of the desired radial force be F_r. In addition, because radial force is proportional to the current square, let $F_r = K_F i_F^2$ for convenience, i.e. i_F is the desired "force current", then

$$i_F^2 = 4KC \tag{15}$$

Using i_T and i_F to represent the desired torque and radial force, then K and C can be found by solving Eqs. (14)-(15) simultaneously, and the result is

$$C = \sqrt{\frac{i_T^2 \pm \sqrt{i_T^4 - (1/8)i_F^4}}{2}} \tag{16}$$

$$K = \frac{i_F^2}{4C} \tag{17}$$

Note that there are two possible solutions for C, and one of them gives negative excitation currents. Although this has no influence on motor torque and radial force generation, it is desirable that all the excitation currents be positive.

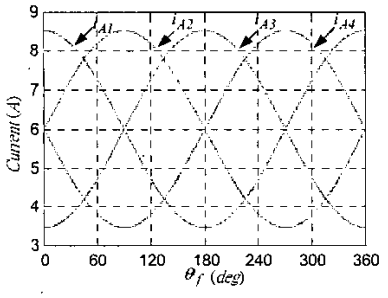

Fig. 3 Excitation currents when i_T = 6A, i_F =7.5 A, θ_r = 5°, and θ_f varied from 0 to 360°

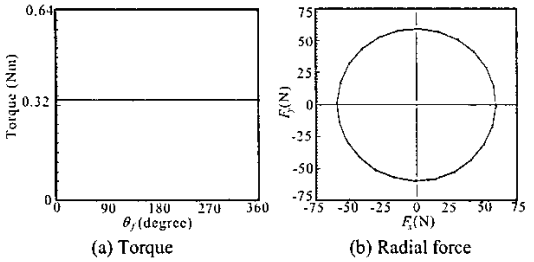

(a) Torque (b) Radial force

Fig. 4 Motor torque and radial force when i_T = 6A, i_F =7.5 A, θ_r = 5°, and θ_f varied from 0 to 360°

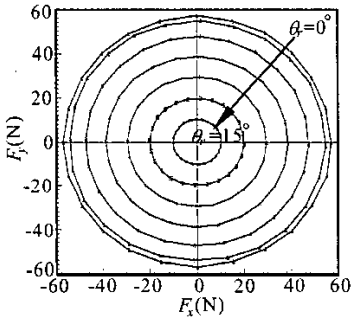

Fig. 5. Radial force when θ_r varied from 0° to 15° and θ_f varied from 0 to 360°

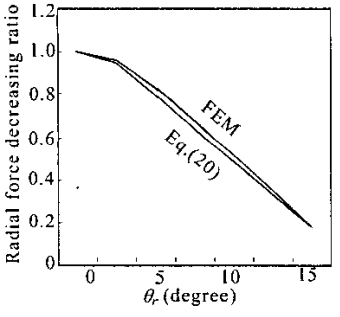

Fig. 6. Comparison of radial force calculated with FEA and with Eq. (20)

The above results were verified with a FEA software. The parameters of the motor used in the calculation are shown in Appendix A. In the calculations, i_T and i_F were set to 6A and 7.5A, respectively, θ_r = 5° (θ_r = 0° is the aligned position), and θ_f varied from 0° to 360°. The calculated excitation currents are shown in Fig. 3, and the motor torque and radial force are shown Fig. 4 (a) and (b), respectively. It can be seen that the amplitude of the radial force does not change as θ_f varied, and its direction is identical to θ_f. Also, as shown in Fig. 4(a), the motor torque is approximately constant when θ_f varied. Note that the torque is small because θ_r is in the neighborhood of the align position.

IV. Radial Force and Torque When Rotor Angle Varies

The results shown in the previous section assumed a fixed rotor angle. In this section, the relationships between radial force and rotor angle are analyzed. As shown in Eq. (4), the electromagnetic force is a function of the overlapping area between the stator and rotor pole tooth, i.e. inversely proportional to rotor angle. But, because the fringing flux was neglected in Eq. (4), the calculated force has significant error in the vicinity of rotor aligned positions. This can be verified with the FEA calculated radial force shown in Fig. 5, where θ_r varied from 0° to 15° with 2.5° increments. The excitation currents are the same as shown in Fig. 3. It can be seen that the radial force changed slightly for θ_r < 2.5°, but decreased almost linearly with the rotor angle for θ_r >2.5°.

When the fringing flux is included, the electromagnetic force produced by pole *A1* can be found from Eq. (1) as

$$F_{A1} = \frac{\mu_0 N^2 i_{A1}^2 LR\theta_o}{2g^2} + \frac{N^2 i_{A1}^2 K_f \theta_{uo}}{2g} \qquad (18)$$

Also, at the aligned position, i.e. θ_o = 15° and θ_{uo} = 0 °, the force is

$$F_0 = \frac{\mu_0 N^2 i_{A1}^2 LR}{2g^2}\left(\frac{\pi}{12}\right) \qquad (19)$$

Dividing Eq. (19) into Eq. (18) yields an expression for the normalized radial force as

$$F_N = \frac{\theta_o}{15} + K_{fg} g \theta_{uo} \qquad (20)$$

where $K_{fg} = \frac{K_f}{\mu_0 LR}\left(\frac{12}{\pi}\right)$, and F_N is the normalized radial force for pole *A1* when the overlapping angle is θ_o. The equation indicates that F_N is not only varies with θ_o but also with θ_{uo}.

It is interesting to note that when all four poles are included, the normalized radial force of phase *A* also equals F_N. This is because all the poles in the phase are perpendicular to one another in space, therefore all the currents cancelled out after Eq. (19) is normalized. For comparison, Fig. 6 shows the radial forces calculated by FEA and by Eq. (20). It can be seen that the two curves are very close to each other. Therefore, Eq. (20) can be used to calculate radial force with good accuracy.

Equation (20) is a very useful supplement to the sinusoidal excitation scheme presented previously. It can be used to calculate the correct current amplitude, i.e. *K*

and C, for the desired radial force at any θ_r. To take a simple example, it is desired to keep the radial force the same as if it were at the aligned position while θ_r varies. To start with the procedures of finding the correct K and C, the normalized force of the present θ_r is calculated with Eq. (20). Then, the desired i_F is multiplied with the normalized force to obtain a new i_F. Finally, Eqs. (16)-(17) with the new i_F and the desired i_T are solved for the current waveforms. Figure 7 shows the radial force calculated with these procedures when θ_r varied from 2.5° to 15° with 2.5° increments. It can be seen that after compensation, the radial force are very close to the desired values when comparing with the θ_r = 0° curve shown in Fig. 5.

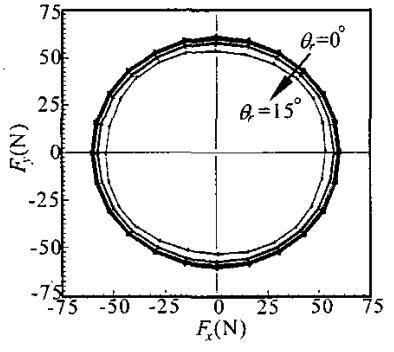

Fig. 7. Radial force with θ_r compensation, θ_r varied from 0° to 15°

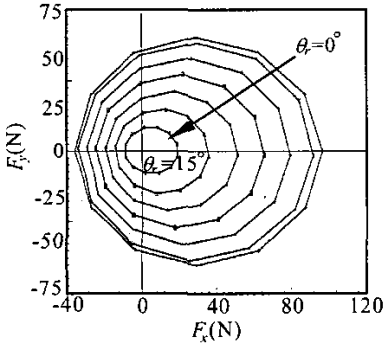

Fig. 8. Radial force when θ_r varied from 0 to 15°, rotor is eccentric in X-direction, d_x= 0.1mm, θ_r is not compensated

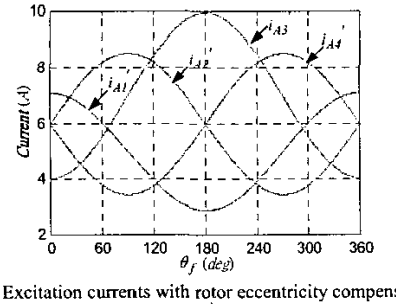

Fig. 9. Excitation currents with rotor eccentricity compensation for θ_r = 0° and d_x= 0.1mm

V. Rotor Eccentricity

Rotor eccentricity has strong influence on the motor radial force. In this section, the effect of eccentricity in one axis is studied. Referring to Fig. 1, consider the case when the rotor is located d_x from the center in the horizontal direction. From Eqs. (5)-(6), only the X-direction force is produced, and it is

$$F_x = K_F\left(\frac{i_{A1}^2}{(g-d_x)^2} - \frac{i_{A3}^2}{(g+d_x)^2}\right) \tag{21}$$

Figure 8 shows the FEA calculated radial force when d_x = 0.1mm and θ_r varied from 0° to 15°, the excitation currents are the same as those shown in Fig. 5. It can be seen that the force in the positive X-direction was amplified while the force in the negative X-direction shrunk due to the eccentricity. This result agreed with the force equation shown in Eq. (21).

Similar to the θ_r compensation presented previously, radial force error due to rotor eccentricity can also be compensated for through the adjustment of excitation currents. Let $i_{A1} \sim i_{A4}$ be the excitation currents that yield the desired motor torque and force when the rotor is not eccentric, and $i_{A1}' \sim i_{A4}'$ be the currents that yield the same torque and force when the rotor is eccentric d_x. From Eqs. (5)-(6) one can obtain the following relationships,

$$\frac{(i_{A1}')^2}{(g-d_x)^2} - \frac{(i_{A3}')^2}{(g+d_x)^2} = \frac{i_{A1}^2}{(g)^2} - \frac{i_{A3}^2}{(g)^2} \tag{22}$$

$$\frac{(i_{A2}')^2}{(g-d_y)^2} - \frac{(i_{A4}')^2}{(g+d_y)^2} = \frac{i_{A2}^2}{(g)^2} - \frac{i_{A4}^2}{(g)^2} \tag{23}$$

Thus, after $i_{A1} \sim i_{A4}$ are found from Eqs. (16)-(17), $i_{A1}' \sim i_{A4}'$ can be solved from the above equations to compensate for the errors due to the rotor eccentricity.

Note that before the adjustment, $i_{A1} \sim i_{A4}$ are identical in shape but different in phase. But after the adjustment, $i_{A1}' \sim i_{A4}'$ do not have to bear the same shape. Figure 9 shows a typical set of adjusted excitation currents, they were calculated with Eqs. (22)-(23) for the θ_r = 0° curve shown in Fig. 8. It can be seen that i_{A2}' and i_{A4}' have the same amplitude since there is no eccentricity in Y-direction. However, i_{A3}' is much greater than i_{A1}' in order to compensate for the rotor eccentricity.

VI. Limitations of the Proposed Schemes

In the preceding sections we have presented a scheme to generate the desired torque and radial force for 12/8 pole SRM. There are several limitations, as given below, must be considered carefully when applying this scheme.

1) When solving Eqs. (16)-(17), K must less than or equal to C so that the resulting currents be sinusoidal. This leads to the following relationship after some simplifications,

$$i_F \le \sqrt[4]{8} \cdot i_T \tag{24}$$

The above relationship provides a limit on the ratio of the attainable radial force and motor torque.

2) The excitation currents can't exceed the motor rated current. In other word, the available motor current limits the maximum attainable radial force. For the motor used in this paper, the maximum radial force circle (as shown in Fig. 5) is only about 4.0 N when it is running ay the rated operating condition.

3) The saturation effect was ignored in the discussion above. Because the motor used in this study was designed to operate in the linear region on purpose, therefore, iron saturation has very little effect on the presented results.

4) Radial force ripple caused by phase commutation are also neglected.

VII. Experimental Verifications

A control system was built to experimentally verify the scheme presented in this paper. The motor shown in Appendix A was used for the experiments. In the experimental setup, the motor was placed vertically to avoid gravitational force, and two load cells are employed to measure the radial force against the motor shaft. Figure 10 shows the schematic of the current controllers and the radial force measurement system. Because only static experiments were performed, i.e. motor was at standstill, only the poles of phase A were excited. Each pole winding has its own current control loop, and a TMS320F240 DSP was used to perform all the current controls. Hysteresis control action was used, and the switching frequency was about 14 KHz.

Because radial force is symmetric to the horizontal and the vertical axis, only the first-quadrant results are shown in the experimental data given below. Figure 11 shows the excitation currents and the measured radial force when θ_r varied form 0° to 15° and θ_f varied form 0° to 90°. The desired radial force and motor torque were set to 27N and 20% rated torque, respectively. The currents were calculated from Eq.(8)-(11), and C and K were found to be 3.0 and 2.0, respectively. Notice the radial force decreased gradually as θ_r increased from 0° to 15°. This agrees with the FEA results shown in Fig. 5.

Figures 12-13 show the excitation currents and radial force, respectively, after the rotor angle effect was compensated. The compensation was based on Eq. (20), and the currents for θ_r = 5°, 10°, and 15° are shown. These results demonstrated the effectiveness of the rotor angle compensation scheme presented in Section IV.

Finally, the rotor was placed about 0.1mm off its center to verify the compensation scheme described in Section V. The direction of the eccentricity was assigned as X-direction for convenience. Figure 14 and 15 show the radial force for various rotor angles before and after, respectively, the rotor eccentricity was compensated using Eq. (22). Note that after the compensation, the radial force was very close to the θ_r = 0° curve shown in Fig. 15.

VIII. Conclusions

In this paper, the radial force and torque produced by a 12/8 SRM under sinusoidal excitations were analyzed, and a scheme to independently control radial force and torque was proposed. It was found that when excited with sinusoidal currents, the SRM is capable of generating the desired shaft radial force in any direction in the rotational plane without interfering with the rotational torque. Some limitations on the proposed sinusoidal excitation scheme were also discussed. The scheme was verified both with FEA software and with experiments. Static experiments were performed, and the results have verified the effectiveness of the proposed scheme in controlling radial force of the SRM.

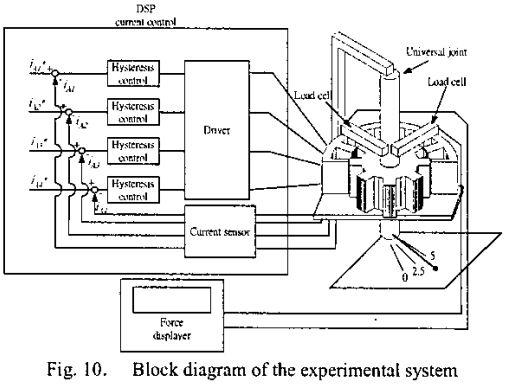

Fig. 10. Block diagram of the experimental system

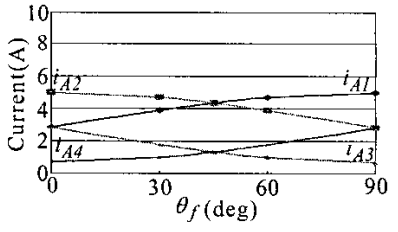

(a) Excitation currents

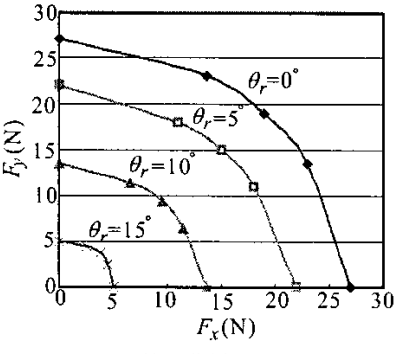

(b) Radial force

Fig. 11. Excitation currents and radial force when θ_r varied from 0° to 15° and θ_f varied from 0 to 90°

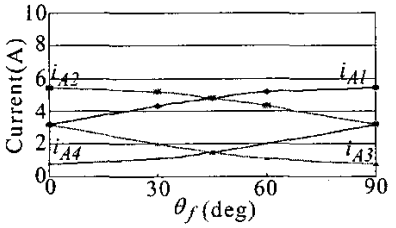

(a) θ_r =5°

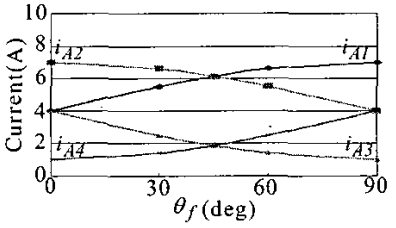

(b) θ_r =10°

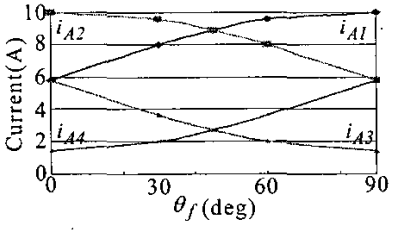

(c) θ_r = 15°

Fig. 12. Excitation currents for various θ_r after θ_r was compensated

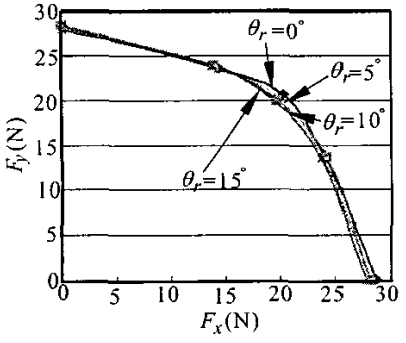

Fig. 13. Radial force for various θ_r after θ_r was compensated

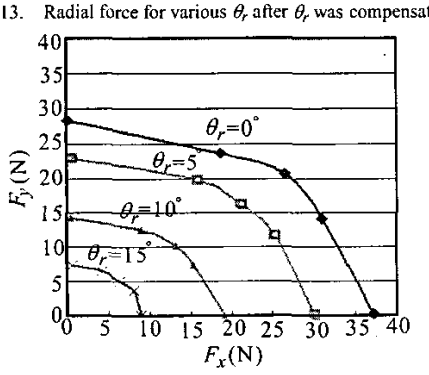

Fig. 14. Radial force for various θ_r when the rotor has 0.1mm eccentricity in X-direction

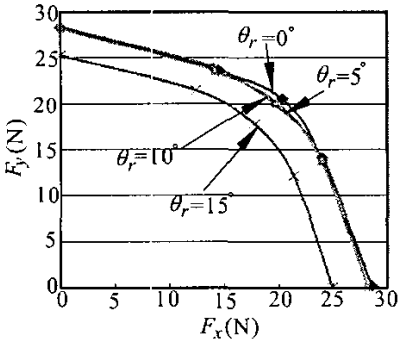

Fig. 15. Radial force for various θ_r after the eccentricity was compensated

APPENDIX A

Parameters of the 12/8 pole SRM are:

output power	1 HP
aligned inductance	8 mH
unaligned inductance	2 mH
rated torque	3 Nm
rated current	10 A

ACKNOWLEDGMENT

We gratefully acknowledge the support for this research by the National Science Council, Taiwan, R. O. C., under grant: NSC 91-2213-E-032-033.

REFERENCE

[1] N.R. Garrigan, W. L. Soong, C. M. Stephens, A. Storace, and T.A. Lipo, "Radial Force Characteristics of a Switched Reluctance Machine", IEEE IAS Annual Meeting, Vol.4, 1999, pp.2250-2258.

[2] I. Husain, A. Radun, and J. Nairus, "Unbalanced Force Calculation in Switched Reluctance Machines", IEEE. Trans. on Magnetics, vol. 36, Jan. 2000, pp. 330-338.

[3] C. Michioka, T. Sakamoto, O. Ichikawa, A. Chiba, and T. Fukao, "A Decoupling Control Method of Reluctance-Type Bearingless Motors Considering Magnetic Saturation", IEEE IAS Annual Meeting, vol.1, Oct. 1995, pp.405-411.

[4] M. Takemoto, H. Suzuki, A Chiba, T. Fukao, and M. A. Rahman, "Improved Analysis of a Bearingless Switched Reluctance Motor", IEEE. Trans. on Industry Applications., vol.37, Jan./Feb. 2001, pp. 26-34.

[5] M Takemoto, A Chiba, H. Akagi, and T. Fukao "Radial Force and Torque of a Bearingless Switched Reluctance Motor Operating in a Region of Magnetic Saturation", IEEE IAS Annual Meeting, vol. 1, 2002, pp. 35-42.

[6] G. R. Slemon, "Electric Machines and Drives", Addison Wesley, 1992.

[7] T. H. Liu, Y. J. Chen, and M. T. Lin, "Vector Control and Reliability Improvement for a Switched Reluctance Motor", IEEE International Conference on Industrial Technology, 5-9 Dec. 1994, pp. 538 -542.

[8] N. J. Nagle, and R. D. Lorenz, "Rotating Vector Method for Sensorless, Smooth Torque Control of a Switched Reluctance Motor Drive", IEEE IAS Annual Meeting, vol.1, 12-15 Oct. 1998, pp. 723 -730